H2 gas production in calcium silicate hydrates: influence of water content and radiation induced defects

Jeremy Haas, Stéphane Esnouf, Jean-Philippe Renault, Adeline Dannoux-Papin, Chengying Yin

INVESTIGATION OF MECHANISMS OF RADIOLYTIC H_2 PRODUCTION IN C-S-H: INFLUENCE OF WATER CONTENT AND RADIATION INDUCED DEFECTS.

YIN C.[1], DANNOUX-PAPIN A.[1], HAAS J.[1], ESNOUF S.[2], RENAULT J-P.[3]

[1]CEA, DES, ISEC, DE2D, SEAD, LCBC, Univ Montpellier, Marcoule, France

[2]Université Paris-Saclay, CEA, Service d'Etude du Comportement des Radionucléides, 91191, Gif-sur-Yvette Cedex, France

[3] Université Paris Saclay, CEA, CNRS, NIMBE, 91191 Gif-sur-Yvette Cedex, France

Abstract: Water radiolysis is a major concern for the conditioning of radioactive waste in cement materials. Synthetic calcium silicate hydrates (C-S-H), the main hydrates of concrete, were synthesized with different calcium to silicate ratios and relative humidity. The samples were irradiated under γ- and electron beam irradiation. The radiolytic hydrogen production was quantified and the radiation induced defect produced at low temperature was characterized by electron paramagnetic resonance. The results show that the radiolytic H_2 production and defect production are 20% sensitive to the relative humidity .

Keywords:

Radiolysis, C-S-H, concrete, adsorbed water, relative humidity

1. INTRODUCTION

Radioactive waste can be classified according to various criteria: origin, physical and chemical nature, level and type of radioactivity, lifetime, etc. In France, radioactive waste is managed according to classification in six categories, which are based on the radioactivity content and the half-life of the waste (figure 1):
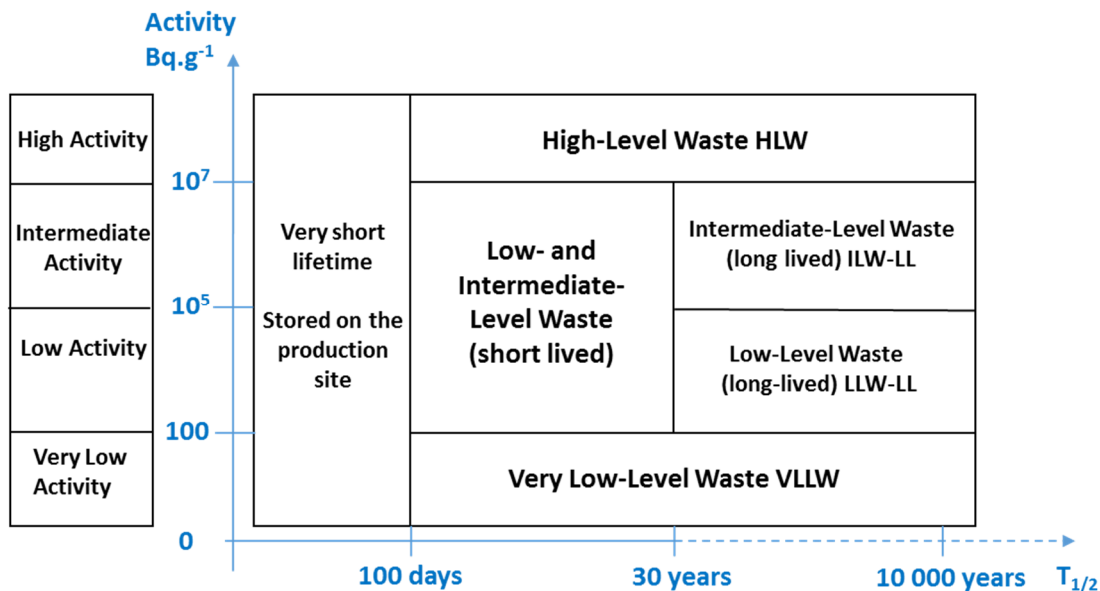

Figure 1. Simplified classification of radioactive waste according to its radioactivity and its half-life. Reproduced from (Lainé 2017).

According to ANDRA's National Inventory of Radioactive Materials and Wastes published at the end of 2020 (Andra 2020), Low- and intermediate-Level short-lived wastes (LILW-SL) accounted for 60 % of the total volume of radioactive wastes produced in France, or 945,000 m³ and 0.03 % of the total radioactivity of radioactive wastes in France. In contrast, the estimated volume of Intermediate-level long lived waste (ILW-LL) is around 43,000 m³. These low and intermediate level wastes, resulting from the decommissioning of nuclear facilities, are usually conditioned in calcium silicate cement to ensure the stability and the confinement of the radioactivity for disposal and future geological storage.

The use of a cement matrix sis prioritized because it offers many advantages: (i) the process and raw materials are inexpensive; (ii) the matrix can be tailored to reach various properties such as stability and strength and (iii) the alkalinity of calcium silicate cements allows the precipitation of

a large number of radionuclides to limit their diffusion (Atkins et al. 1992). However, the ionizing radiations emitted by the waste lead to dihydrogen release, which has to be quantified and minimized for the safety of nuclear disposal. (Bonin et al. 2000, Chartier et al. 2018)

The cement paste is mainly composed of calcium silicate hydrates (abbreviated C-S-H[1]) (about 60 % - 70 %) and calcium hydroxide (portlandite mineralogic phase). In such hydrates, the H_2 source is either structural hydroxyls, adsorbed water or pore water (Kaddissy et al. 2017, Kaddissy et al. 2019). Since it is a material with various possible compositions and a complex nano- and micro-structure (Allen et al. 2007, Pellenq et al. 2009), the radiolytic process leading to hydrogen release in such a material is challenging and not well understood. Although the behaviour of cement paste under irradiation has been studied in the literature (Bibler 1980) (Bouniol et al. 2008) (Ewing et al. 1995, Allen et al. 2007, Bouniol et al. 2008, Bouniol et al. 2013, Dezerald et al. 2015, Le Caër et al. 2017) (Chartier et al. 2018) (Acher 2017), only few data related to the H_2 gas production of C-S-H are available (Yin et al. 2019) (Acher 2017). An enhancement of H_2 production in C-S-H compared to bulk water and an increase of the yield with the specific surface has been established. The impact of relative humidity (RH) does not seem to have been studied, even though the morphology of C-S-H and distribution of water in the solid are strongly affected by RH and even though RH will increase with time, due to the exchange of water with the wet host geological medium. Structural investigations of these hydrates by SAXS and Neutron scattering have shown (Allen et al. 1982) (Thomas et al. 1998) (Allen et al. 1987) that the average number of stacking layers increases with the water content, from 4.5 (with 10 % water content) to 11 (with 30 % water content) (Chiang et al. 2012) and the total thickness of one nanoparticle ranges from 4 to 10 nm (Figure 2). These observations are corroborated by atomic force microscopy that gives for those C-S-H nanoparticles 30-60 nm^2 surface and 5 nm thickness (Nonat 2004).

---

[1] The general formula is $(CaO)_x (SiO_2)_y (H_2O)_z$ with CaO/SiO_2 (abbreviated C/S) varying from 0.66 to 2.
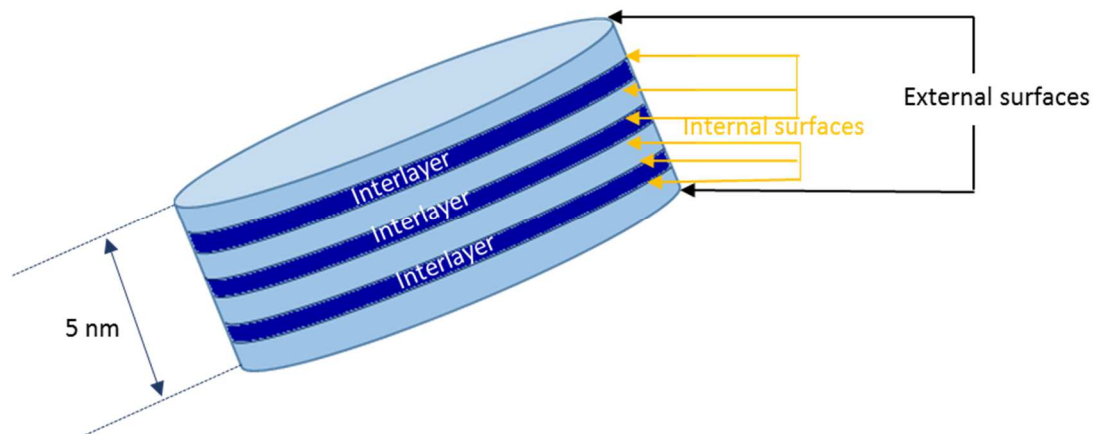
Figure 2. Schematic of a C-S-H nanoparticle.

Based on the structural model presented in figure 2, four types of water can be described in C-S-H gels (Roosz et al. 2016): the structural hydroxyl groups contained in the layers (0.08-0.1 g/g of dried C-S-H, depending on the calcium to silica ratio), the water confined in the interlayer space (0.12 g/g that decreases upon heating under vacuum), the water adsorbed on the external surface of the nanoparticle (0.04 to 0.4 g/g of dried C-S-H, depending on the RH) and the water condensed in the pores between the nanoparticles (for RH> 90%). However, in the practical range of hygrometry and temperature used in storage, only adsorbed water and pore water contents are expected to vary.

We tried here to go further than a mere quantification of H_2 production by linking it to the various primary species produced under irradiation using a low temperature analysis. Our main purpose was to identify the H_2 precursor and the oxidative counterpart to H_2 production that remains trapped in the material, as no O_2 is usually produced under irradiation of hydrates.

2. MATERIALS AND METHODS

2.1 Synthesis of C-S-H

C-S-H samples were synthesized from reaction of amorphous silica (SiO_2, AEROSIL 380, Degussa) and calcium oxide (CaO) in excess of water. Reagent grade calcium carbonate ($CaCO_3$, VWR Company) was calcined at 960 °C for 24 hours to obtain calcium oxide. Stoichiometric amounts of CaO and SiO_2 were mixed in order to produce C-S-H samples having an initial C/S ratio of 1.6. The materials were mixed with ultrapure water (Milli-Q 18 MΩ) with a water to solid mass ratio of 50 in 1 L sealed bottles. Then, they were shaken on a rotating rack for 1 month at room

4

temperature (*i.e.* 25°C) to obtain equilibrium. Then, samples were filtered using a Büchner funnel and a filter paper (0.22 μm, Millipore) and rinsed. Usually, solid sample is rinsed with an organic solvent to obtain pure samples. In our study, this step was prohibited in order to avoid the presence of organic compounds, which would give a supplementary contribution to radiolytic H_2 production.

The concentrations of remaining calcium and silicon ions in the filtered solutions were determined by ICP-AES.

The samples were freeze-dried during 4 days and then they were cured in a desiccator chamber at 30%, 60%, 75%, and 85% relative humidity (RH) under a nitrogen atmosphere at room temperature until their weight stabilized (approximatively 4 weeks). The relative humidity was controlled by saturated salts: 30% RH with Magnesium Chloride, 60% RH with Sodium Bromide, 75% RH with Sodium Chloride and 85% RH with Potassium Chloride.

2.2 Sample Characterization

The characterization methods (X ray diffraction, thermogravimetric analysis and electron paramagnetic resonance) are described in the supporting information.

2.3 Sample chemical composition

The experimental C/S ratios were indirectly checked by the chemical analysis of the solution at the end of the synthesis as previously described (Yin et al. 2019). The pH values and [CaO], [SiO_2] in solution according to C/S ratio indicate that samples were at equilibrium according to the solubility curve (Flint 1934) (Roller et al. 1940) (Taylor 1950) (Greenberg et al. 1965) (Grutzeck et al. 1989) (Lecoq 1993) (Cong et al. 1996)

2.4 Irradiation experiments and gas analysis

C-S-H samples were γ-irradiated using a ^{60}Co source experimental irradiator at Marcoule (Gammatec, Steris, France). Approximately 120 mg were introduced in 12 mL Pyrex glass ampules, which were then flame-sealed under argon at about 900 mbar to avoid oxygen presence. Attention has been paid to avoid modifying the water content of the samples during

the sealing, which has been confirmed by TGA measurements. Glass ampules were placed on a rotating plate to ensure the spatial homogeneity of the dose delivery. Dosimetry was performed with red Perspex dosimeters and the absorbed dose is known with a 5.6 % standard deviation. Samples were irradiated by using an average dose rate of 600 Gy/h at 25 ± 1°C up to 100 and 200 kGy of absorbed doses. For each absorbed dose, two independent samples were irradiated.

The amount of dihydrogen produced during γ-irradiation was evaluated by using a micro-gas chromatography (490 Micro-GC, Agilent) equipped with a compression system (SRA Instruments) to provide 1 bar of pressure at the input of the μ-GC injector. The channel used for hydrogen analysis contains a Molecular Sieve 5A PLOT column under argon at 28 psi pressure and a micro thermal conductivity detector (μ-TCD). The oven and detector temperatures were respectively 90 and 120 °C, with an acquisition time of 2 minutes.

The hydrogen production yield, denoted as the G-value and expressed in mol/J, corresponds to the amount of dihydrogen produced per amount of absorbed energy. For each C-S-H sample, apparent hydrogen radiolytic yield $G(H_2)$ was assessed by calculating the slope of the hydrogen production as a function of the absorbed dose. Normalized apparent hydrogen radiolytic yields $G_{norm}(H_2)$, expressed in mol/J, were calculated by normalizing apparent hydrogen radiolytic yields by the initial water mass fraction, which was measured. The standard deviation of the yields was estimated to be less than 15 %.(see table S1)

Electron beam irradiations were used for EPR experiments. The C-S-H samples were irradiated at 77K using a linear accelerator located in NIMBE, Saclay, France. The pulse-width was 10 ns and the electron energy was 10 MeV and the repetition rate was 5 Hz. No sample heating was detected. The typical dose delivered per pulse determined using the Fricke dosimeter was 6 Gy/pulse.

3. RESULTS

3.1 X-Ray powder Diffraction

The purity of C-S-H samples was controlled by X-Ray powder Diffraction (XRD). An example of a characteristic XRD pattern is presented in supporting figure S2. The X ray diffraction pattern is completely compatible with our previous results. (Yin et al. 2019)

In short, the experimental patterns show that the samples present the diffraction peaks corresponding to the tobermorite structure (Grangeon et al. 2013), a natural mineral analogue of C-S-H, and additional peaks are attributed to a small amount of calcium hydroxide (portlandite phase) and calcium carbonate (calcite phase). The appearance of portlandite is probably due to the further hydration process during the storage, because of possible residual water after lyophilisation. Calcite is commonly found in C-S-H since it is known to react with CO_2 from the atmosphere. In our case, carbonation of the samples most likely occurred in the desiccators. The interlayer distance in the tobermorite phase is determined by the position of the (001) peak (between 6 and 10° in the 2theta scale) using the structural model described by Grangeon et al. (Grangeon et al. 2013) (see figure 3).
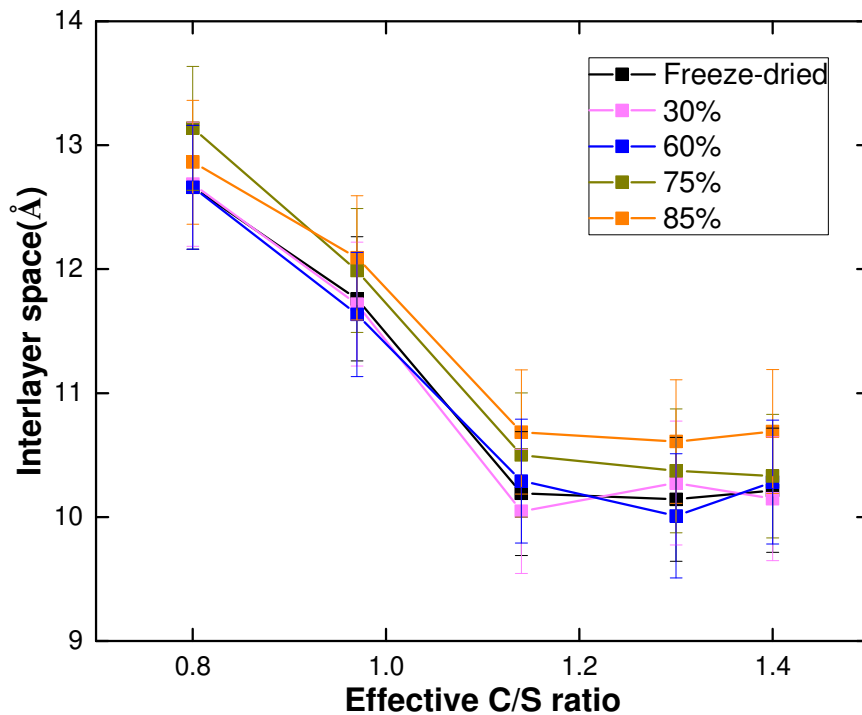
Figure 3. Interlayer space of C-S-H samples deduced from XRD patterns as a function of the C/S ratio at different RH. The error on the d_{001} value is estimated at 0.5 Å (Holmboe et al. 2012).

According to (Gaboreau et al. 2020), the values of d_{001} in the 10-13 Å range correspond to a simple water layer separating the C-S-H foils, the decrease in distance with the increase in C/S arising from the omission of Si tetrahedral combined with the insertion of Ca^{2+} in the interlayers space. Whatever the C/S ratio, the layer-to-layer distance decreases slightly (0.5 Å) with the

relative humidity, as already observed by Cong (Cong et al. 1995) and Gaboreau (Gaboreau et al. 2020). This decrease corresponds most probably to a change of the water content in the interlayer, leading to a local shrinkage. However, the decrease is too limited, even at low RH, to consider that the interlayer space is empty of water molecules (Gaboreau et al. 2020).

3.2 Thermogravimetry analysis

An example of a characteristic thermogram is presented in Fig. S1B. Three steps of decomposition are observed. The first one, from 30 to 300°C, corresponds to the loss of the sum of pore water, crystallization water and hydroxides (Taylor 1986). The second step, from 410 to 500°C, corresponds to the decomposition of few amounts of portlandite ($Ca(OH)_2$) (Krakowiak et al. 2015). In the third step, the weight loss from 550 to 750°C, results from the decomposition of carbonates. Note that temperature boundaries are approximate and depend on the heating rate and on how the water interacts with solid surfaces.

A typical result of the TGA analysis is given in Table 1. The amount of water sensitive to the RH is of about 5% of the total water.

Table 1. Typical water, portlandite and calcite contents calculated from thermogravimetry analysis of 1.40 C-S-H samples cured at different relative humidity. The relative uncertainty is estimated to be 10%.

	Water content (%)	Portlandite (%)	Calcite (%)
Freeze-dried	14.2	5.8	3.5
30%	17.3	7.7	3.3
60%	16.9	4.7	4.2
75%	18.5	3.3	4.7
85%	20.8	3.0	2.6

Chemically Bonded Water (CBW, *i.e.* crystallization water and structural water) and Free Water (FW) which corresponds to water molecules more weakly bonded, were calculated according to (Taylor 1986) (Lainé et al. 2017) (Le Caër et al. 2017): free water weight loss occurs between ambient and 105°C while chemically bonded water weight loss occurs between 105°C and

highest temperature (1000°C). In order to simplify the interpretation, we considered CBW only between 105 and 300°C.

Figure 4 (and the complementary figure S3 and table S2) shows the distribution of CBW and FW of C-S-H samples with 1.3 C/S ratio cured at different RH. As expected, our results show that the chemically bonded water content is almost constant, within the error bars, whereas free water increases with relative humidity. This validates a posteriori our treatment. Free water (FW) is also observed for freeze-dried samples, as it is already observed in clays (Lainé et al. 2017). This result confirms that freeze-dried samples are very sensitive to the surrounding environment (CO_2, RH)(Li 2011). According to the molecular formula of the corresponding tobermorite phases (11 Å phase, ($Ca_5Si_6O_{16}(OH)_2 \cdot 5H_2O$) (Galvánková et al. 2016) (Richardson 2014)) and the analysis of Roosz et al. (Roosz et al. 2016), the CBW content corresponds to a single layer of water adsorbed in the interlayer. This result is coherent with the interlayer space measurements presented in §3.1. In this latter interpretation, the FW content (5-15%) corresponds to water adsorbed on the external surface of the nanoparticle presented in Figure 2.
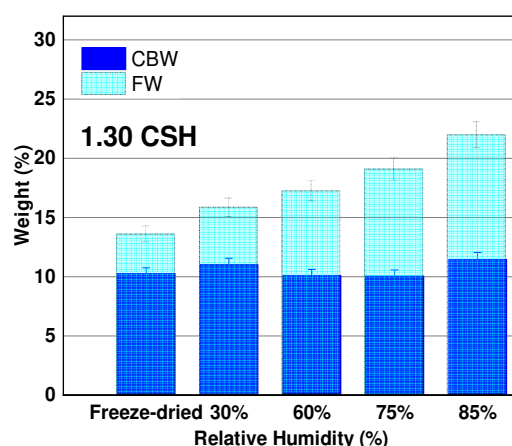
Figure 4. Typical percentage of free water (FW) and chemically bound water (CBW) as determined from TGA measurements in sample 1.30 C-S-H as a function of relative humidity. Other C/S ratio are presented in figure S3

3.3 Hydrogen production under gamma irradiation

An example of the evolution of H_2 as a function of dose is given in Figure 5**.** The quantity of H_2 produced increases linearly with the dose. The radiolytic yields for each sample, at each RH, was deduced from the slopes of the lines. The yields were calculated either with respect to the total

mass of C-S-H and water, considering the total energy deposited in the whole system, or with respect to the energy received solely by water.
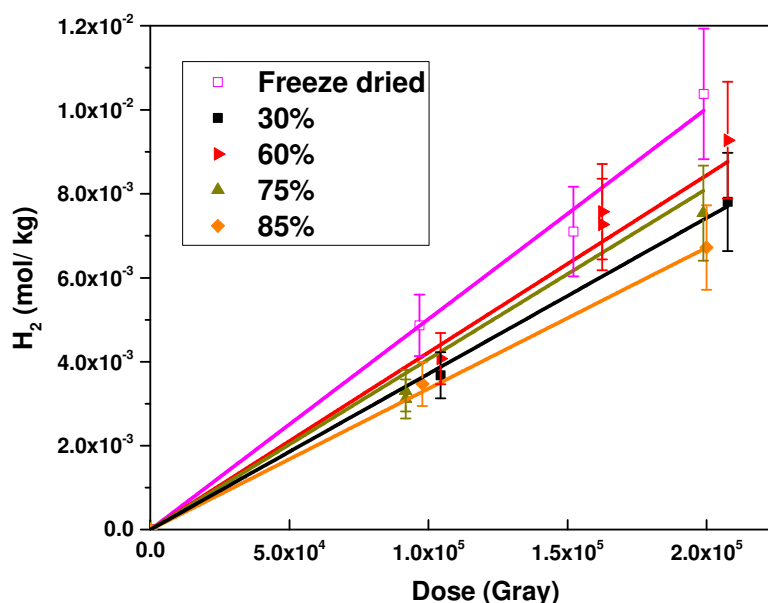

Figure 5. Dose dependence of H_2 production for hydrated 1.30 C-S-H equilibrated **at** different relative humidity at room temperature (freeze-dried, 30, 60, 75 and 85 % RH).

Table 2, Table 3 and Figure 6 present hydrogen production under gamma irradiation from various C-S-H as a function of water content. When calculated with respect to the total amount of material (Table 2), the G values vary from 0.35×10^{-7} mol J^{-1} to 0.7×10^{-7} mol J^{-1}. In agreement with our previous measurements, G values tend to decrease when the C/S ratio increases (Yin et al. 2019). The yields are comparable to the one measured in bulk water (0.45×10^{-7} mol J^{-1}) showing that C-S-H produce the same quantity as an equivalent mass of bulk water. Figure 6 and table 2 show that G values vary by less than 20% with various water content, to be compared to a relative error of 15% (see table S1). Therefore it is difficult to affirm that the water content have a significant effect on H_2 production. The same trend was reported in Ca^{2+} exchanged-Montmorillonites (Fourdrin et al. 2013), where the raw $G(H_2)$ is almost constant for all RH.

10

This result highlights a great efficiency of the radiolysis of –OH groups (both for FW and CBW) and of the recombination of hydrogen atoms. The $G(H_2)$ of C-S-H is very close to the $G(H_2)$ of cement paste S3 (S3 is mainly composed of C-S-H, about 93%) reported by Le Caër (Le Caër et al. 2017). On the contrary, distinctive tendencies were noticed for Na exchanged Montmorillonites (Na^-MX80, Na-Mt) and geopolymers (Geo-Na, Geo-K, Geo-Cs), where the raw $G(H_2)$ increases with water content (Fourdrin et al. 2013) (Chupin et al. 2017) or for synthetic montmorillonite, where $G(H_2)$ decreases with water content (Lainé et al. 2017). The marginal role of the amount of water on G values is traditionally interpreted through ultraefficient energy transfer phenomena from the solid to the liquid (Le Caër et al. 2005, Rotureau et al. 2005).

Indeed, in our case, energy transfer processes can appear as an increase of the yield calculated with respect to the amount of energy received by water, when the water content decreases (see Table 3). However, the value presented in Table 3 must be used carefully, as they can also hide the radiolytic events that can occur within the material. Therefore, for practical applications, we can simply consider that the solid produces hydrogen with the same efficiency as the liquid. It means also that, simple drying strategies that do not remove structural water may not be efficient to decrease significantly H_2 production in C-S-H. Unfortunately, treatments that remove structural water (*i.e.* heating under vacuum) are prohibited, as the material integrity may be affected.

Table 2. Hydrogen radiolytic yields (10-7 mol/J) (calculated with respect to the total energy received by the system) released from Gamma irradiated C-S-H samples with different C/S ratio hydrated at different RH at room temperature. The standard deviation of the yields are estimated to be 15% for all samples.

$G(H_2)$ (mol/J×10^{-7}) (calculated with respect to the total energy received by the system)		Real C/S ratio				
		0.80	0.97	1.14	1.30	1.40
RH (%)	f.d.	0.52±0.08	0.56±0.08	0.46±0.07	0.50±0.08	0.32±0.05
	30%	0.69±0.10	0.39±0.06	0.44±0.07	0.37±0.06	0.35±0.06
	60%	0.61±0.10	0.58±0.09	0.49±0.07	0.42±0.07	0.36±0.06

	75%	0.66±0.10	0.61±0.10	0.44±0.07	0.41±0.06	0.35±0.06
	85%	0.62±0.10	0.62±0.10	0.46±0.07	0.34±0.05	0.35±0.06

Table 3. Hydrogen radiolytic yields (10^{-7} mol/J) (calculated with respect to the energy received solely by water) released from Gamma irradiated C-S-H samples with different C/S ratio hydrated at different RH at room temperature. The standard deviations of the yields are estimated to be 15% for all samples.

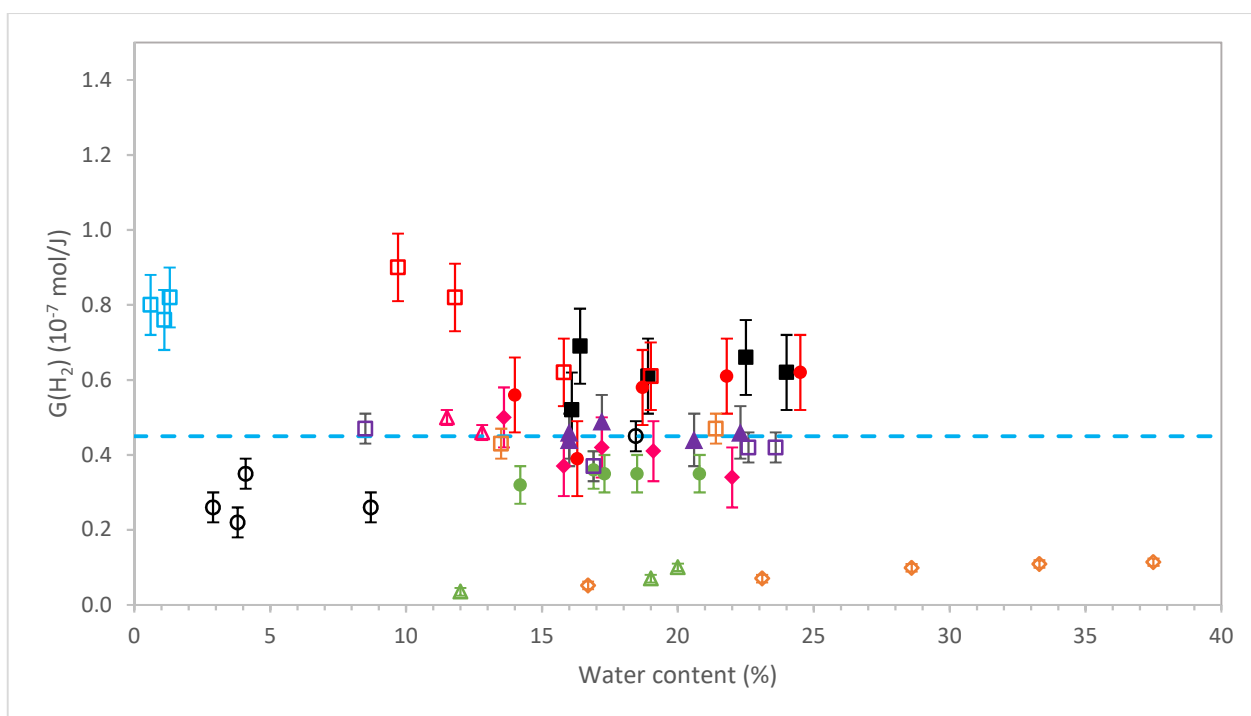| $G_{norm.}$ (H$_2$) (mol/J×10^{-7}) (calculated with respect to the energy received solely by water)		Real C/S ratio				
		0.80	0.97	1.14	1.30	1.40
RH (%)	3%	3.2±0.5	4.0±0.6	2.9±0.4	3.7±0.6	2.3±0.3
	30%	4.2±0.6	2.4±0.3	2.8±0.3	2.3±0.2	2.0±0.3
	60%	3.2±0.5	3.1±0.5	2.8±0.4	2.4±0.4	2.1±0.3
	75%	2.9±0.4	2.8±0.4	2.1±0.3	2.1±0.3	1.9±0.3
	85%	2.6±0.4	2.5±0.5	2.1±0.3	1.5±0.2	1.7±0.3

Figure 6. Correlation between the water content obtained from TGA and G(H$_2$) for different nanotructured materials. This work (■ 0.80 C-S-H, ● 0.97 C-S-H, ▲ 1.14 C-S-H, ◆ 1.30 C-S-H, ● 1.40 C-S-H), ☐ Na exchanged montmorillonite (Na$^+$-MX80) (Fourdrin et al. 2013), ☐ calcium exchanged montmorillonite (Ca^{2+}-Mt) (Fourdrin et al. 2013), △ geopolymer (Geo Na) (Chupin et al. 2017), Boehmite (⬭ ALOOH S and ☐ ALOOH L) (Kaddissy et al. 2019)☐ Synthetic Montmorillonite (Lainé et al. 2017), ◇ Portland Ultimat CEM I (Chartier et al. 2018), △ cement paste S3 (Le Caër et al. 2017), – – – bulk water).

We point out that the primary G value of bulk water (in Figure 6) is measured with the addition of potassium bromide to prevent the back reaction of oxidative radicals with dihydrogen (Schwarz et al. 1954) (Schwarz 1955), allowing the measurement of the primary G value of bulk water at room temperature. The C-S-H themselves can produce efficient dihydrogen whatever the calcium content, that is to say, there are some species, which can behave like storage site of oxidative radicals in these hydrates.

3.4 Radiation induced defects

Considering that in materials containing hydroxyl groups, the transient oxidative species can be stored in paramagnetic radiation induced defects (RIDs), (Kaddissy et al. 2019) we conducted a quantification of the paramagnetic species induced by irradiation by electron paramagnetic

We checked that gamma irradiation did not lead to modification of the crystallographic properties, *i.e.* that only radiation induced defects (RID) were created, even at 200 kGy (figure S4).
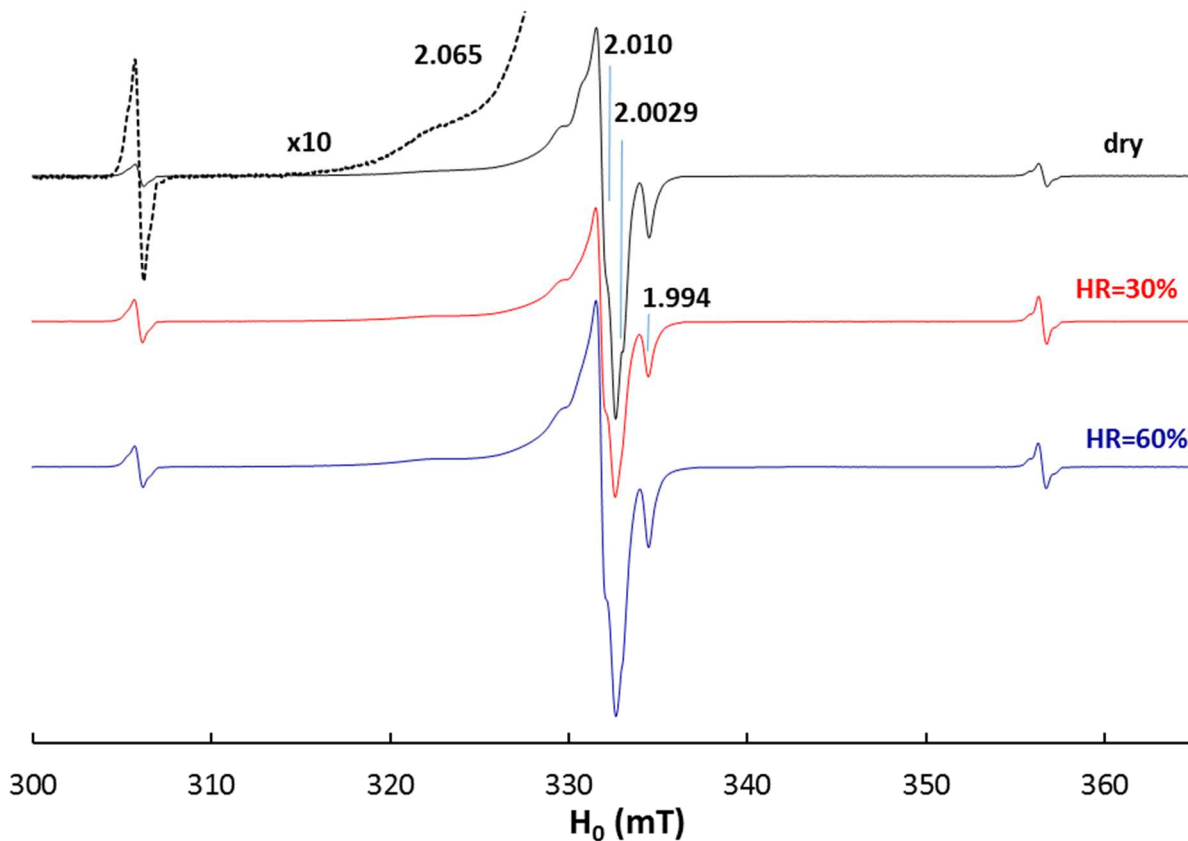
Figure 7. EPR spectra of electron irradiated at 77 K of 0.80 C-S-H with different relative humidity, irradiated at 30 kGy.

Figure 7 presents the EPR spectra of electron irradiated at 77 K of C-S-H with C/S=0.80 with different relative humidity. The results evidence that there is minimal differences when the relative humidity varies from 3% (freeze-dried) to 60%. These results are in accordance with the measurements of hydrogen gas production and show that adsorbed water has a minimal effect on irradiation primary processes. Owing to these similarities , we will describe together RIDs for the different relative humidities.

A doublet separated by 50 mT assigned to H radicals is observed in all C-S-H samples (Kaddissy et al. 2019). The hyperfine constant is very close to that for free H atom (50.8 mT).

14

The signal presents also the signature of a superhyperfine coupling, with two shoulders separated by 1.3 mT, indicating weak interactions of the H atom with its surrounding. (Päch et al. 1997) The rest of the ESR spectrum is composed of a complex, central line centered around g=2.010. This line presents a broad shoulder, hereafter designed as RID I, around g=2.065 for C-S-H 0.80, 0.97 and 1.30 and g=2.044 for C-S-H 1.14 and 1.40 (fig. S5). According to similar distributions that have been reported for hole centers trapped in alkali aluminosilicate or silicate glasses (Table S3), we assign this defect to a $O^\bullet$ center.

A narrow singlet line with g=2.0029 is attributed either to carbon contamination (Griscom et al. 1999) or to different type of oxygen hole center (Dutt et al. 1991).

The high field signal corresponding to g=1.994 reveals an anisotropic signal (called RID II in the following). From the comparison with various published results in table S3, this signal is attributed to an O_2^- species. It can come from the following reactions:

$$O^{-\bullet} + O^{-\bullet} \rightarrow O_2^{2-} \qquad \text{(Eq. 1)}$$

$$O_2^{2-} + O^{-\bullet} \rightarrow O_2^- + O^{2-} \qquad \text{(Eq. 2)}$$

Similar reactions can be found in the general scheme of basic water radiolysis (El Omar et al. 2015), and are indeed the deprotonated counterpart to the ones proposed in hyperquenched glassy water to explain the efficient production of superoxide (Bednarek et al. 1996).

Table 4. Concentration and yield in radiation induced defects for different RH and C/S ratios. The experimental accuracy is estimated to be ±35%. Hydrogen radiolytic yields released from Gamma irradiated C-S-H samples at room temperature are recalled. f.d. stands for freeze dried C-S-H.

C/S ratio	0.80	0.80	0.80	0.97	1.14	1.30	1.40
RH	f.d.	30%	60%	f.d.	f.d.	f.d.	f.d.
H atoms (/g)	$1.3\ 10^{16}$	$2.4\ 10^{16}$	$2.4\ 10^{16}$	$2.0\ 10^{16}$	$5.4\ 10^{15}$	$8.5\ 10^{15}$	$4.4\ 10^{15}$
RID (/g)	$1.4\ 10^{18}$	$1\ 10^{18}$	$1.5\ 10^{18}$	$1.6\ 10^{18}$	$1.5\ 10^{18}$	$5.4\ 10^{17}$	$1.4\ 10^{18}$
G(RID I+II) (mol/J×10^{-7})	0.81	0.6	0.85	0.89	0.82	0.60	0.81
G(H$_2$) (mol/J×10^{-7})	0.52	0.69	0.61	0.56	0.46	0.50	0.32

(calculated with respect to the total energy received by the system)						

The formation of both H radicals and O^- centers (RID I) points towards the existence of homolytic dissociation process that are only marginally affected by water.

$$R \cdots OH \rightarrow R \cdots O^{\bullet} + H^{\bullet} \qquad \text{(Eq. 3)}$$

The ratio G(RID I+II)/G(H_2) between 1 and 2 suggest also that H° recombination (Eq. 4) is the natural source of hydrogen (H_2)

$$H^{\bullet} + H^{\bullet} \rightarrow H_{2\,released} \qquad \text{(Eq. 4)}$$

As a minor competing reaction, the formed H atoms can also be trapped :

$$H^{\bullet} \rightarrow H^{\bullet}_{trapped} \qquad \text{(Eq. 5)}$$

The competition between H atom recombination (Eq. 4) and trapping (Eq. 5) explain why the concentration of $H_{trapped}$ is lower than the concentration in RIDs(table 4), whose recombination is less efficient at this temperature

The amount of H trapped increases slightly (Table 4) with the water content whereas RID I and II remain the same considering the experimental errors. This indicates that adsorbed water at low temperature provides additional H trapping sites.

In a second time, we studied also the stability of the different radiation damage with temperature. RID I decreases with the temperature and converts into RID II. This confirms that RID II comes from RID I recombination through equations 1 and 2. After annealing at 280 K (Figure S6), the shape of the signal is very close to those observed in pure irradiated portlandite in the same condition, but with the intensity is 10 times smaller. EPR spectrum is the superposition of different lines tentatively attributed to O_2^-, O_3^- and CO_2^-.
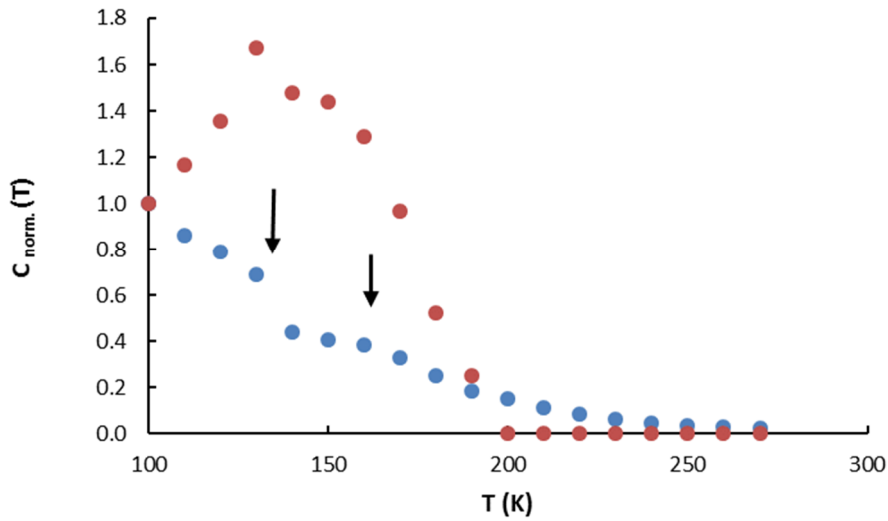
Figure 8. Temperature evolution of the total intensity of EPR spectra related to RID I (blue points) and RID II (red points).

Therefore, we attribute these signals to residual radicals trapped in the portlandite phase of our samples. The radiation induced defects formed in the C-S-H themselves disappear completely at room temperature. This is a strong difference with the observations in hydroxides and oxohydroxides (Kaddissy et al. 2017), where the H and RID were stable at room temperature, RID providing in this case the oxidative counterpart to H_2 production. A correlation of this behaviour is that the oxidative counterpart to H_2 remains also unknown in C-S-H, but peroxide and oxygen are the most probable oxidized products (Eq. 6).

$$O_2^- + O_2^- \rightarrow O_2^{2-} + O_2 \qquad \textbf{(Eq. 6)}$$

Indeed, calcium peroxide has been proposed as a major product in irradiated concrete (Bouniol et al. 2012). However, no oxygen production as ever been observed in irradiated concrete or C-S-H. This raises the interesting question of the actual solubility of O_2 in the interlayer space.

We point out that no evidence in our results allows proposing that the radiation events leading to defect formation occur more within the material or within the water (adsorbed or interlayer). The only indication we have is the low temperature recombination of H and RIDs, suggesting that these radiation induced defects are formed in mobile environment, *i.e.* near water. As

17

observed in photocatalysis on amorphous materials, the water would therefore play a critical role in stabilizing radiogenerated charge carriers (Litke et al. 2017, Shirai et al. 2018).

4. CONCLUSIONS

The production of radiolytic dihydrogen of different C-S-H samples has been quantified and shows a limited effect of the relative humidity on the radioytic yields. The arising radiation induced defects have been identified as H° atoms, $O^{-\circ}$ and O_2^- centers at 77K, but disappear at room temperature. Their formation points toward a direct radiolysis of material OH bonds.

5. REFERENCES

.
Acher, L. (2017). Investigation of the behaviour of cement matrices and their hydrates under γ and electron irradiation. PhD, Université Paris Saclay

Allen, A., R. Oberthur, D. Pearson, P. Schofield and C. Wilding (1987). "Development of the fine porosity and gel structure of hydrating cement systems." Philosophical Magazine B **56**(3): 263-288.

Allen, A., C. Windsor, V. Rainey, D. Pearson, D. Double and N. M. Alford (1982). "A small-angle neutron scattering study of cement porosities." Journal of Physics D: Applied Physics **15**(9): 1817.

Allen, A. J., J. J. Thomas and H. M. Jennings (2007). "Composition and density of nanoscale calcium–silicate–hydrate in cement." Nature materials **6**(4): 311-316.

Andra (2020). "National Inventory of Radioactive Materials and Waste."

Atkins, M. and F. Glasser (1992). "Application of Portland cement-based materials to radioactive waste immobilization." Waste management **12**(2-3): 105-131.

Bednarek, J., A. Plonka, A. Hallbrucker, E. Mayer and M. C. R. Symons (1996). "Hydroperoxyl Radical Generation by γ-Irradiation of Glassy Water at 77 K." Journal of the American Chemical Society **118**(39): 9387-9390.

Bibler, N. E. (1980). Radiolytic Gas Generation in Concrete Made with Incinerator Ash Containing Transuranium Nuclides. Scientific Basis for Nuclear Waste Management. C. J. M. Northrup. Boston, MA, Springer US**:** 585-592.

Bonin, B., M. Colin and A. Dutfoy (2000). "Pressure building during the early stages of gas production in a radioactive waste repository." Journal of Nuclear Materials **281**(1): 1-14.

Bouniol, P. and E. Bjergbakke (2008). "A comprehensive model to describe radiolytic processes in cement medium." Journal of Nuclear Materials **372**(1): 1-15.

Bouniol, P. and S. Lapuerta-Cochet (2012). "The solubility constant of calcium peroxide octahydrate in relation to temperature; its influence on radiolysis in cement-based materials." Journal of Nuclear Materials **420**(1): 16-22.

Bouniol, P., B. Muzeau and V. Dauvois (2013). "Experimental evidence of the influence of iron on pore water radiolysis in cement-based materials." Journal of Nuclear Materials **437**(1): 208-215.

Chartier, D., J. Sanchez-Canet, L. Bessette, S. Esnouf and J. P. Renault (2018). "Influence of formulation parameters of cement based materials towards gas production under gamma irradiation." Journal of Nuclear Materials **511**: 183-190.

Chiang, W.-S., E. Fratini, P. Baglioni, D. Liu and S.-H. Chen (2012). "Microstructure determination of calcium-silicate-hydrate globules by small-angle neutron scattering." The Journal of Physical Chemistry C **116**(8): 5055-5061.

Chupin, F., A. Dannoux-Papin, Y. N. Ravache and J.-B. d. E. de Lacaillerie (2017). "Water content and porosity effect on hydrogen radiolytic yields of geopolymers." Journal of Nuclear Materials **494**: 138-146.

Cong, X. and R. J. Kirkpatrick (1995). "Effects of the temperature and relative humidity on the structure of C-S-H gel." Cement and Concrete Research **25**(6): 1237-1245.

Cong, X. and R. J. Kirkpatrick (1996). "29Si MAS NMR study of the structure of calcium silicate hydrate." Advanced Cement Based Materials **3**(3-4): 144-156.

Dezerald, L., J. J. Kohanoff, A. A. Correa, A. Caro, R. J. M. Pellenq, F. J. Ulm and A. Saúl (2015). "Cement As a Waste Form for Nuclear Fission Products: The Case of 90Sr and Its Daughters." Environmental Science and Technology **49**(22): 13676-13683.

Dutt, D., P. Higby, C. Merzbacher and D. Griscom (1991). "Compositional dependence of trapped hole centers in gamma-irradiated calcium aluminosilicate glasses." Journal of non-crystalline solids **135**(2-3): 122-130.

El Omar, A. K., G. Baldacchino, I. Monnet and P. Bouniol (2015). "Revisited water radiolysis at elevated pH by accounting O3˙− kinetics at low and high LET." RSC Advances **5**(108): 89244-89253.

Ewing, R. C., W. J. Weber and F. W. Clinard (1995). "Radiation effects in nuclear waste forms for high-level radioactive waste." Progress in Nuclear Energy **29**(2): 63-127.

Flint, E. (1934). "Study of the system CaO-SiO_2-H_2O at 30℃ and of the reaction of water on the anhydrous calcium calcium silicates." J. Research NBS **12**: 751.

Fourdrin, C., H. Aarrachi, C. Latrille, S. Esnouf, F. Bergaya and S. Le Caër (2013). "Water radiolysis in exchanged-montmorillonites: the H2 production mechanisms." Environmental science & technology **47**(16): 9530-9537.

Gaboreau, S., S. Grangeon, F. Claret, D. Ihiawakrim, O. Ersen, V. Montouillout, N. Maubec, C. Roosz, P. Henocq and C. Carteret (2020). "Hydration Properties and Interlayer Organization in Synthetic C-S-H." Langmuir **36**(32): 9449-9464.

Galvánková, L., J. Másilko, T. Solný and E. Štěpánková (2016). "Tobermorite Synthesis Under Hydrothermal Conditions." Procedia Engineering **151**: 100-107.

Grangeon, S., F. Claret, C. Lerouge, F. Warmont, T. Sato, S. Anraku, C. Numako, Y. Linard and B. Lanson (2013). "On the nature of structural disorder in calcium silicate hydrates with a calcium/silicon ratio similar to tobermorite." Cement and Concrete Research **52**: 31-37.

Greenberg, S. A. and T. N. Chang (1965). "Investigation of the Colloidal Hydrated Calcium Silicates. II. Solubility Relationships in the Calcium Oxide-Silica-Water System at 25°C." The Journal of Physical Chemistry **69**(1): 182-188.

Griscom, D. L., C. I. Merzbacher, R. A. Weeks and R. A. Zuhr (1999). "Electron spin resonance studies of defect centers induced in a high-level nuclear waste glass simulant by gamma-irradiation and ion-implantation." Journal of Non-Crystalline Solids **258**(1): 34-47.

Grutzeck, M., A. Benesi and B. Fanning (1989). "Silicon‐29 magic angle spinning nuclear magnetic resonance study of calcium silicate hydrates." Journal of the American Ceramic Society **72**(4): 665-668.

Holmboe, M., S. Wold and M. Jonsson (2012). "Porosity investigation of compacted bentonite using XRD profile modeling." Journal of Contaminant Hydrology **128**(1-4): 19-32.

Kaddissy, J. A., S. Esnouf, D. Durand, D. Saffre, E. Foy and J.-P. Renault (2017). "Radiolytic Events in Nanostructured Aluminum Hydroxides." The Journal of Physical Chemistry C **121**(11): 6365-6373.

Kaddissy, J. A., S. Esnouf, D. Saffré and J.-P. Renault (2019). "Efficient hydrogen production from irradiated aluminum hydroxides." International Journal of Hydrogen Energy **44**(7): 3737-3743.

Krakowiak, K. J., J. J. Thomas, S. Musso, S. James, A.-T. Akono and F.-J. Ulm (2015). "Nano-chemo-mechanical signature of conventional oil-well cement systems: Effects of elevated temperature and curing time." Cement and Concrete Research **67**: 103-121.

Lainé, M. (2017). Etude du comportement de matériaux argileux sous rayonnement ionisant. PhD, Université Paris-Saclay.

Lainé, M., E. Balan, T. Allard, E. Paineau, P. Jeunesse, M. Mostafavi, J. L. Robert and S. Le Caër (2017). "Reaction mechanisms in swelling clays under ionizing radiation: influence of the water amount and of the nature of the clay mineral." RSC Advances **7**(1): 526-534.

Le Caër, S., L. Dezerald, K. Boukari, M. Lainé, S. Taupin, R. M. Kavanagh, C. S. N. Johnston, E. Foy, T. Charpentier, K. J. Krakowiak, R. J. M. Pellenq, F. J. Ulm, G. A. Tribello, J. Kohanoff and A. Saúl (2017). "Production of H2 by water radiolysis in cement paste under electron irradiation: A joint experimental and theoretical study." Cement and Concrete Research **100**(Supplement C): 110-118.

Le Caër, S., P. Rotureau, F. Brunet, T. Charpentier, G. Blain, J. P. Renault and J.-C. Mialocq (2005). "Radiolysis of Confined Water: Hydrogen Production at a High Dose Rate." ChemPhysChem **6**(12): 2585-2596.

Lecoq, X. (1993). Etude de l'hydratationa concentration controlee du silicate tricalcique et des caracteristiques de ses produits de reaction. PhD, Dijon.

Li, Z. (2011). Advanced concrete technology, John Wiley & Sons.

Litke, A., Y. Su, I. Tranca, T. Weber, E. J. M. Hensen and J. P. Hofmann (2017). "Role of Adsorbed Water on Charge Carrier Dynamics in Photoexcited TiO2." The Journal of Physical Chemistry C **121**(13): 7514-7524.

Nonat, A. (2004). "The structure and stoichiometry of C-S-H." Cement and Concrete Research **34**(9): 1521-1528.

Päch, M. and R. Stösser (1997). "Scavenger Assisted Trapping of Atomic Hydrogen in Si8O12-Cages." The Journal of Physical Chemistry A **101**(44): 8360-8365.

Pellenq, R. J.-M., A. Kushima, R. Shahsavari, K. J. Van Vliet, M. J. Buehler, S. Yip and F.-J. Ulm (2009). "A realistic molecular model of cement hydrates." Proceedings of the National Academy of Sciences **106**(38): 16102-16107.

Richardson, I. G. (2014). "Model structures for C-(A)-S-H(I)." Acta crystallographica Section B, Structural science, crystal engineering and materials **70**(Pt 6): 903-923.

Roller, P. S. and G. Ervin Jr (1940). "The system calcium oxide-silica-water at 30. the association of silicate* ion in dilute alkaline solution." Journal of the American Chemical Society **62**(3): 461-471.

Roosz, C., S. Gaboreau, S. Grangeon, D. Prêt, V. Montouillout, N. Maubec, S. Ory, P. Blanc, P. Vieillard and P. Henocq (2016). "Distribution of Water in Synthetic Calcium Silicate Hydrates." Langmuir **32**(27): 6794-6805.

Rotureau, P., J. P. Renault, B. Lebeau, J. Patarin and J. C. Mialocq (2005). "Radiolysis of confined water: molecular hydrogen formation." Chemphyschem **6**(7): 1316-1323.

Schwarz, H. A. (1955). "The Effect of Solutes on the Molecular Yields in the Radiolysis of Aqueous Solutions1." Journal of the American Chemical Society **77**(19): 4960-4964.

Schwarz, H. A., J. P. Losee and A. O. Allen (1954). "Hydrogen Yields in the Radiolysis of Aqueous Solutions1." Journal of the American Chemical Society **76**(18): 4693-4694.

Shirai, K., G. Fazio, T. Sugimoto, D. Selli, L. Ferraro, K. Watanabe, M. Haruta, B. Ohtani, H. Kurata, C. Di Valentin and Y. Matsumoto (2018). "Water-Assisted Hole Trapping at the Highly Curved Surface of Nano-TiO2 Photocatalyst." Journal of the American Chemical Society **140**(4): 1415-1422.

Taylor, H. F. (1986). "Bound water in cement pastes and its significance for pore solution compositions." MRS Online Proceedings Library Archive **85**.

Taylor, H. W. (1950). "726. Hydrated calcium silicates. Part I. Compound formation at ordinary temperatures." Journal of the Chemical Society 3682-3690.

Thomas, J. J., H. M. Jennings and A. J. Allen (1998). "The surface area of cement paste as measured by neutron scattering: evidence for two CSH morphologies." Cement and Concrete Research **28**(6): 897-905.

Yin, C., A. Dannoux-Papin, J. Haas and J. P. Renault (2019). "Influence of calcium to silica ratio on H2 gas production in calcium silicate hydrate." Radiation Physics and Chemistry **162**: 66-71.